Fig. 2. Appearance of **10** as a function of time. Initial concentrations are [**2**] = [**6**] = 8.0 mM in CHCl$_3$. Triethylamine (12 equivalents) was present in all of the reaction solutions. Error bars represent standard deviations of multiple independent runs. (a) Reaction of **2** and **6** without additive. (b) Reaction of **2** and **6** with 0.28 equivalent of **10** added.

observed on adding 0.28 equivalent of the product **10** (Fig. 2). It is an inactive recombinant.

The differences in reactivity of **9** and **10** can be related to the orientations of their respective recognition surfaces. In **9** these can achieve a parallel arrangement. The molecule behaves as a template and can attract **1** and **5** in a productive termolecular complex **11**, poised for intramolecular coupling (Eq. 3). The initial reaction product is the hydrogen-bonded cyclic dimer of **9**. Dissociation of this dimer then results in the increasing concentrations of template that provide the autocatalytic effect.

The hybrid **10** is composed of two U-shaped modules—the Kemp triacid (**8**) and the xanthene diacid (**9**). Its overall configuration is either C-shaped, in which its recognition surfaces converge (**10**, Eq. 4), or S-shaped, in which its recognition surfaces diverge (as in **12**). Neither case allows a productive termolecular complex to be assembled. Nor can the molecule form a hydrogen-bonded cyclic dimer; instead, its self-complementarity is expressed by forming chains.

Self-complementarity is also a common feature of macromolecules, and the orientation of the recognition surfaces within these structures determines the nature of the assemblies that are formed. When these surfaces permit the formation of a dimer, replication is possible (2). Even dynamic systems such as micelles are capable of self-assembly and replication (10). With carefully fixed recognition elements, the assembly of synthetic self-complementary structures into predictable, closed surfaces that encapsulate molecules—or reaction events—of an appropriate scale should be possible (11).

REFERENCES AND NOTES

1. J. I. Hong, Q. Feng, V. Rotello, J. Rebek, Jr., *Science* **255**, 848 (1992).
2. J. Nowick, Q. Feng, T. Tjivikua, P. Ballester, J. Rebek, Jr., *J. Am. Chem. Soc.* **113**, 8831 (1991).
3. V. Rotello *et al.*, *ibid.*, p. 9422.
4. T. K. Park, Q. Feng, J. Rebek, Jr., *ibid.*, in press.
5. All new compounds were characterized by high-resolution mass spectrometry and infrared and nuclear magnetic resonance spectroscopy. Details will be published elsewhere.
6. For autocatalytic effects in the coupling of nucleic acid analogs, see G. von Kiedrowski, *Angew. Chem. Int. Ed. Engl.* **98**, 932 (1986); W. S. Zielinski and L. E. Orgel, *Nature* **327**, 346 (1987); G. von Kiedrowski, B. Wlotzka, J. Helbing, M. Matzen, S. Jordan, *Angew. Chem. Int. Ed. Engl.* **30**, 423 (1991).
7. For example, the acceleration of the initial coupling rate for the case shown in Fig. 1 is 35 ± 5% for only 0.07 equivalent added product and 35% for 0.05 equivalent added product at 4 mM reactants. For replicators **3** and **7** in CHCl$_3$ (a solvent in which template effects are enhanced), three to five times as much product was required before comparable rate increases were observed.
8. D. S. Kemp and K. S. Petrakis, *J. Org. Chem.* **46**, 5140 (1981).
9. J. Nowick, P. Ballester, F. Ebmeyer, J. Rebek, Jr., *J. Am. Chem. Soc.* **112**, 8902 (1990).
10. P. A. Bachmann, P. Walde, P. L. Luisi, J. Lang, *ibid.* **113**, 8204 (1991).
11. The dimer **9** is such a structure. For progress elsewhere on this front, see R. G. Barr and T. J. Pinnavaia, *J. Chem. Phys.* **90**, 328 (1986); M. C. Etter, Z. Urbanczyk-Lipkowska, D. A. Jahn, J. S. Frye, *J. Am. Chem. Soc.* **108**, 5871 (1986); M. Simard, D. Su, J. D. Wuest, *ibid.* **113**, 4696 (1991).
12. We thank the National Science Foundation for support of this research, J. I. Hong for experimental assistance, and G. Joyce for advice.

22 January 1992; accepted 31 March 1992

Reproducible Imaging and Dissection of Plasmid DNA Under Liquid with the Atomic Force Microscope

H. G. Hansma, J. Vesenka, C. Siegerist, G. Kelderman, H. Morrett, R. L. Sinsheimer, V. Elings, C. Bustamante, P. K. Hansma

Reproducible images of uncoated DNA in the atomic force microscope (AFM) have been obtained by imaging plasmid DNA on mica in *n*-propanol. Specially sharpened AFM tips give images with reproducible features several nanometers in size along the DNA. Plasmids can be dissected in propanol by increasing the force applied by the AFM tip at selected locations.

Scanning probe microscopes such as the AFM (*1, 2*) can be used at near-ambient conditions and can yield even atomic resolution on some surfaces (*3*). If this high resolution can be obtained on DNA there could be many benefits, including the potential for sequencing DNA. Until now, however, high-resolution AFM images of DNA have been difficult to reproduce.

Recently Vesenka *et al.* (*4*) and Bustamante *et al.* (*5*) developed a method for anchoring and imaging plasmids that gives reproducible images with mean apparent plasmid widths on the order of 10 to 15 nm. We report here an improvement of this technique that shows reproducible structure along the DNA strands and can resolve detail that is in some cases the size of the double helix. This method may have applications in diverse fields ranging from protein–nucleic acid interactions to chromosome mapping.

Double-stranded plasmids [BlueScript II

H. G. Hansma, G. Kelderman, H. Morrett, R. L. Sinsheimer, P. K. Hansma, Department of Physics, University of California, Santa Barbara, CA 93106.
J. Vesenka, C. Siegerist, C. Bustamante, Institute of Molecular Biology, University of Oregon, Eugene, OR 97403–1229.
V. Elings, Digital Instruments, Inc., 6780 Cortona Drive, Santa Barbara, CA 93117.

from Stratagene, La Jolla, California and pSK 31, a gift from W. Rees at the University of Oregon, Eugene, Oregon (*5*)] were attached to mica treated with magnesium acetate. This method (*6*) builds on earlier methods for imaging DNA on mica in the electron microscope (*7, 8*). DNA on mica was stored over desiccant and then imaged under *n*-propanol in a Nanoscope II AFM (*9*) at constant force mode by using narrow (120- or 200-μm) silicon nitride cantilevers with integrated tips (*10*). The scan speed was typically 9 Hz, or 1 min per image. Good DNA images were easily obtained, although it was sometimes a challenge to get a plasmid distribution over the sample that was neither too sparse nor too dense.

Imaging plasmids under propanol (Fig. 1, A to E) gives better resolution of detail along the strands and narrower apparent widths than imaging in air (Fig. 1F). Propanol was chosen as a medium for imaging based on previous results in air and ethanol. Imaging forces in air are typically on the order of ten times greater than imaging forces in liquids such as ethanol (*11, 12*). Therefore it is desirable to image DNA under liquid to obtain images under the most gentle conditions. Ethanol had been

chosen previously (13) because the insolubility of DNA in ethanol should help keep the DNA on the substrate. However, DNA, at least the short oligomers imaged previously (13), moved around in the AFM experiments under ethanol. DNA is even less soluble in propanol, which was chosen for these experiments. Propanol has the added advantage that, having a low dielectric constant (20.1 at 25°C), it does not significantly screen the electrostatic forces holding the molecules on the mica substrate. Moreover, like other alcohols, propanol is a dehydrating agent that may help expose the molecular surface of the DNA to the probing tip. Both n-propanol and isopropanol, as well as n-butanol, have given comparable images of DNA; stable images have been obtained in aqueous solutions containing as little as 10% propanol.

The reproducibility and stability of the detail along the DNA strand can be seen in Fig. 2. A 120-nm by 120-nm region at the bottom of the plasmid in Fig. 2A was scanned continuously for 10 to 15 min. The last image captured (Fig. 2C) is almost identical to the first (Fig. 2B) except for some drift, and both images show the same bumps with 3- to 5-nm spacing that can be detected in the image of the entire plasmid (Fig. 2A). The apparent width of this plasmid is ~3 nm, comparing favorably with the expected width of 2.4 nm for double-stranded DNA, although apparent widths of 4 to 8 nm are more common (Fig. 1). Zooming in to a smaller scan size reveals somewhat more detail (Fig. 2D), but at smaller scan sizes, the DNA is more easily damaged. This 50-nm by 50-nm zoom of the same region of the plasmid was captured several minutes after the image in Fig. 2C. Since the DNA is in propanol, one would not expect it to have the standard double helix of B-DNA that is seen in aqueous solution. Upon dehydration, B-DNA changes to A-DNA, which has a smaller helix pitch (14). Another question about these images is the extent to which bound water or ions are being imaged instead of the DNA molecule itself. The background spots, many of which change from image to image, are probably salts and can be reduced by washing with water, but this also removes DNA. Also, in the absence of an internal size standard, calibrations are accurate to only several percent. Nonetheless, these AFM images of uncoated DNA molecules show features such as the lumps in Fig. 2, B to D, that appear to be higher order twisting of the DNA strands. Some supercoiling is also evident in Fig. 1, C and E. The relaxed state of most plasmids is probably due to single-strand breaks.

In contrast to plasmids under propanol, plasmids imaged in air show almost no reproducible structure along the strand

(Fig. 1F) (4, 5). Why are the plasmid images so much better in propanol? One answer lies in the AFM force curves (Fig. 3), which show a much smaller adhesion between the sample and the tip in propanol than in air. Force curves differ from the normal AFM imaging mode; the tip, when

generating force curves, is at a fixed xy position and is moved up and down in the z direction, thus moving alternately away from and toward the sample. The shape and position of the curve give information about the imaging force and the degree to which the tip adheres to the sample. The
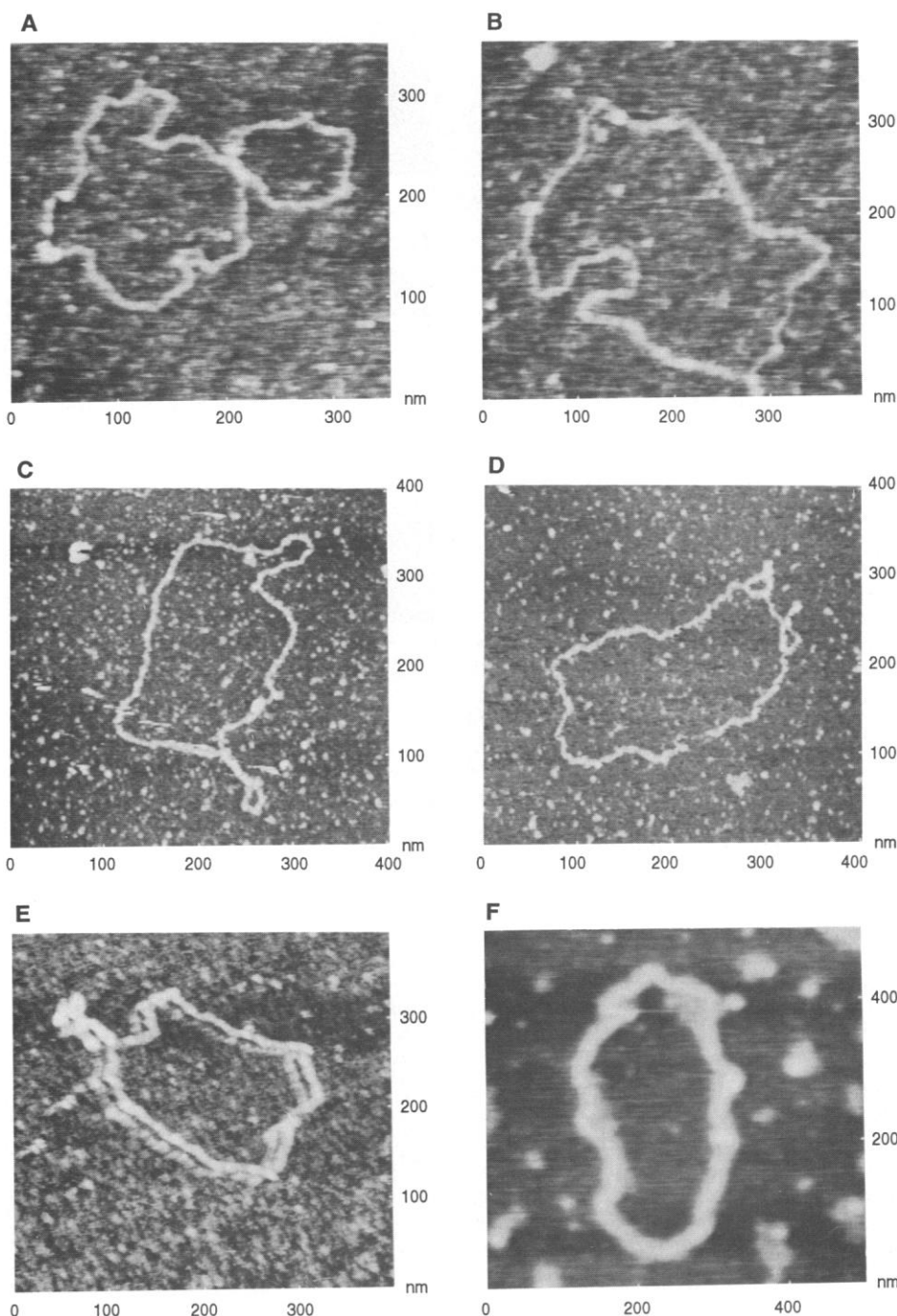
Fig. 1. AFM images of plasmids in propanol (**A** to **E**) and air (**F**). Images (A), (B), and (F) are of plasmids pSK 31; (C) to (E) are of BlueScript II plasmids. Images (A) to (D) were obtained with super tips deposited in the scanning electron microscope (SEM) that were subsequently ion-milled. Image (E) was obtained with a regular pyramidal tip, which was a double tip, as revealed by the double image it produced. Image (F) was obtained with an SEM-deposited super tip that was not ion-milled. Plasmid strands are 3 to 6 nm wide in (A) to (D), and 15 to 20 nm in (F). Image sizes are: (A) 360 nm by 360 nm; (B to E) 400 nm by 400 nm; and (F) 500 nm by 500 nm. The images have been processed only by flattening to remove background slope.

Fig. 2. Plasmids can be scanned repetitively without damage. BlueScript II plasmid was imaged with an ion-milled super tip under propanol at a scan frequency of 4.3 Hz. (**A**) AFM image of entire plasmid molecule. The elongated object in the middle of the plasmid is the convolution of the tip with a large piece of debris (probably a salt crystal), because objects with the same shape and orientation were seen scattered through the images taken with this tip. Thus this tip that gave unusually narrow DNA images was actually a wide tip with one short, fine projection at the end. Scan size 310 nm by 310 nm. (**B**) A 120-nm by 120-nm scan of lower central region of plasmid. (**C**) Scan of same region of plasmid after 10 to 15 min of continuous scanning of this region. Note similarity of plasmid detail between (B) and (C). (**D**) A 50-nm by 50-nm scan of the central region of (C) several minutes after capturing the image in (C). The images have been processed only by flattening to remove background slope.

BlueScript II plasmid

Plasmid detail, first image

Plasmid detail, 15 minutes later

Smaller plasmid detail

force curve in propanol (Fig. 3A) shows little or no hysteresis; the tip pulls away from the sample cleanly without adhering to it. The imaging force calculated from this force curve is ~1 nanonewton (nN), from the product of the 5-nm cantilever deflection and the spring constant of 0.2 nN/nm for the 120-μm narrow cantilever that was used.

The force curve in air shows a larger imaging force and a large hysteresis (Fig. 3B). The large hysteresis indicates that in air the tip adheres strongly to the substrate and can be withdrawn from it only with difficulty. In air, even at 40% humidity, which is used for imaging plasmids, there are traces of water on the tip and the sample, which creates a large meniscus force (*12*, *15*) that perhaps deforms and distorts the DNA enough to obscure detail along the strands and give the DNA a somewhat greater apparent width.

Another factor affecting image quality is the AFM tip (Fig. 4). There seems to be a correlation between tip width and the apparent width of DNA in AFM images (*4*, *5*, *16*), and the shape of the tip convolutes with the shape of the DNA in producing the image. Three different types of AFM tips were used to produce the images in Figs. 1 and 2. The plasmid in Fig. 1F was imaged with a super tip made by depositing a carbide needle onto a standard pyramidal silicon nitride tip with the scanning electron microscope (SEM) (*17*). The plasmids in Fig. 1, A to D, and Fig. 2 were scanned with SEM-deposited super tips that had been sharpened by ion milling. STM tips have also been sharpened by ion milling (*18*). The plasmid in Fig. 1E was scanned with the standard pyramidal tip of Fig. 4A. Standard tips are generally worse for imaging DNA than SEM-deposited super tips. Ion milling produces super tips that are, on
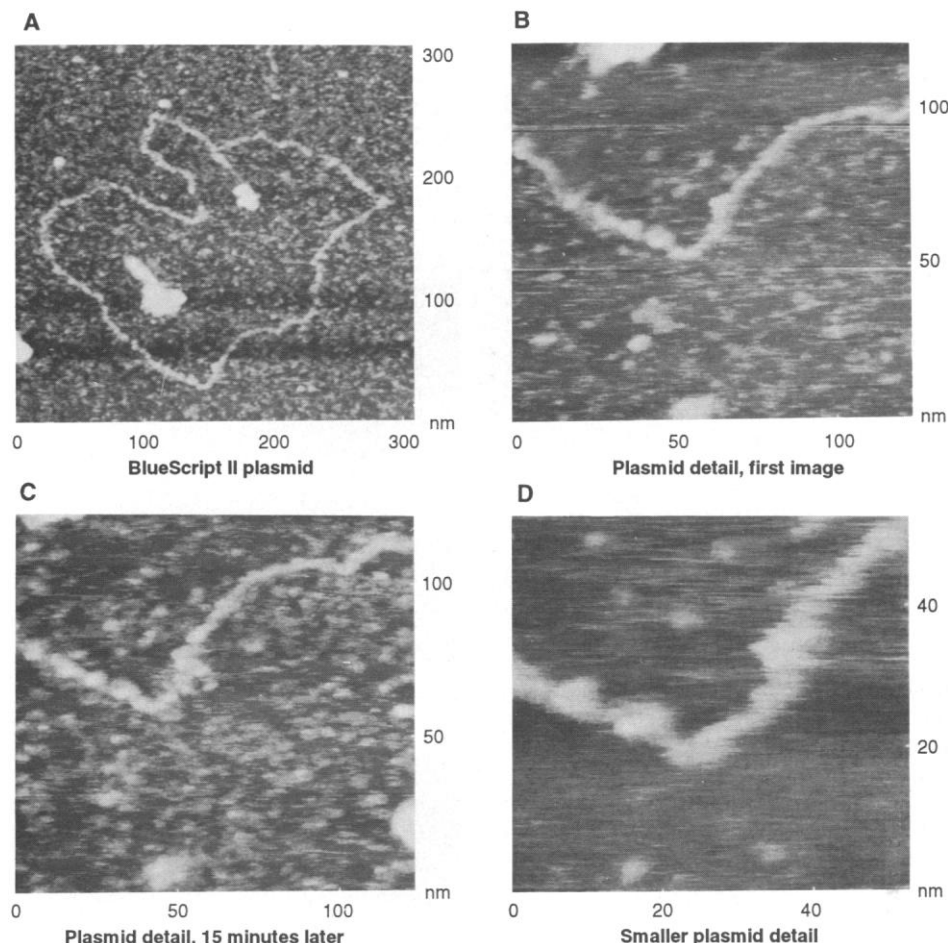
the average, better than non–ion-milled super tips, but there is great variability in the quality of both kinds of super tips; of the

two plasmids with the narrowest apparent widths, one was imaged with a non–ion-milled super tip, whereas the other (Fig. 2)

Fig. 3. AFM force curves in propanol (**A**) and air (**B**). Tip deflection in millivolts (*y*-axis) versus distance between tip and sample in nanometers (*x*-axis). Inset circles show the relative positions of tip and sample at different regions of the force curves. The force curve in propanol (A) lacks the adhesive component seen in air. The tip, at a fixed *xy* position above the sample, is moving up and down in the *z*-direction to generate these curves. The position of the curves along the *x*-axis is arbitrary. The two curves in each graph show the approach (solid line) and the withdrawal (dashed line) of the tip from the sample. The zero on the *y*-axis shows the

cantilever deflection at which imaging will be done after returning to the imaging mode; curves can be shifted in the *y*-direction by changing the set point voltage. The imaging force after returning to the AFM imaging mode is the product of cantilever deflection, measured from the force curve, times the spring constant of the cantilever. These force curves are typical for super tips.
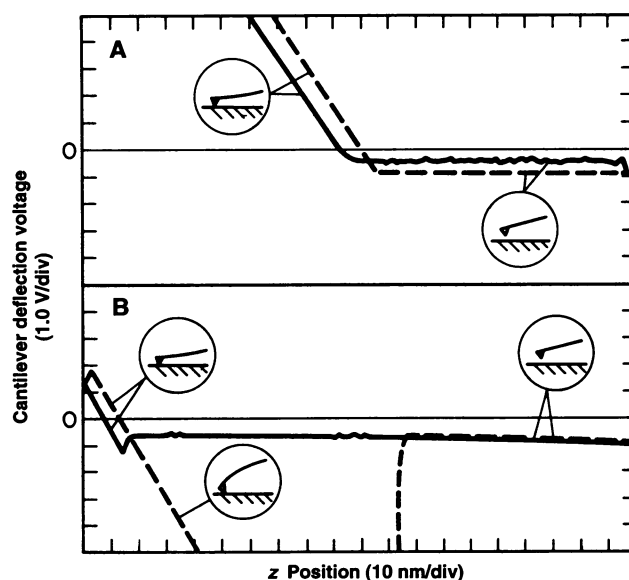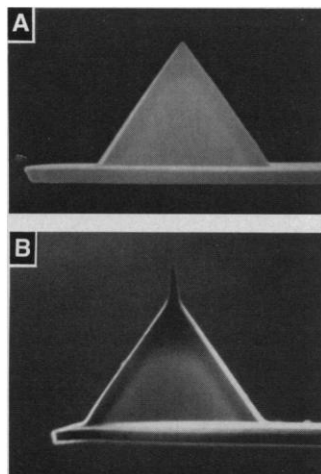
Fig. 4. Scanning electron micrographs of AFM tips. (**A**) Normal pyramidal AFM tip, integrated into silicon nitride cantilever. (**B**) Super tip of contamination deposited onto normal tip in the SEM. This tip has also been sharpened by ion milling (2 min, 2.5 keV argon, 0.5 mA/mm², 10°) and was used for imaging DNA before this picture was taken. Width of the pyramidal tip at the base is 5 μm.

was imaged with an ion-milled super tip. Obtaining reproducible tips is currently a major challenge, especially since good tips often become dull or dirty after 1 day or less of imaging. Images produced by double or triple tips are not uncommon; at present, even our two kinds of super tips have about a 30% probability of being double tips. Although originally regarded as defective, multiple tips may actually be a great boon to high-resolution imaging of DNA by increasing the amount of information in a single image. A comparison of structural detail between the multiple tip images would help to distinguish DNA fine structure from tip artifacts.

Finally, it is possible not only to image but also to manipulate DNA in propanol with the same scanning probe. For example, if the force is increased in small scans, the DNA can be cut, both in air (4, 19) and in propanol (Fig. 5). By increasing the force 5 nN in a 30-nm by 30-nm scan area, a piece of DNA ~1 kb long was scraped away, where it piled up at the left side of the cut (Fig. 5B). Shorter lengths of DNA can be cut away by disabling the scan in the y-direction (4, 19). DNA is more easily dissected in a 80:20 propanol-water mixture than in propanol alone. By making two small cuts at selected regions of the DNA molecule, a section of the molecule can be excised. In order to recover the excised piece of DNA, mica squares of 400 μm or less can be lifted out of the mica surface, and DNA can be removed from mica with water. The question remains whether one can locate and use the cut DNA piece or pieces, which have ends of an unknown chemistry, are accom-
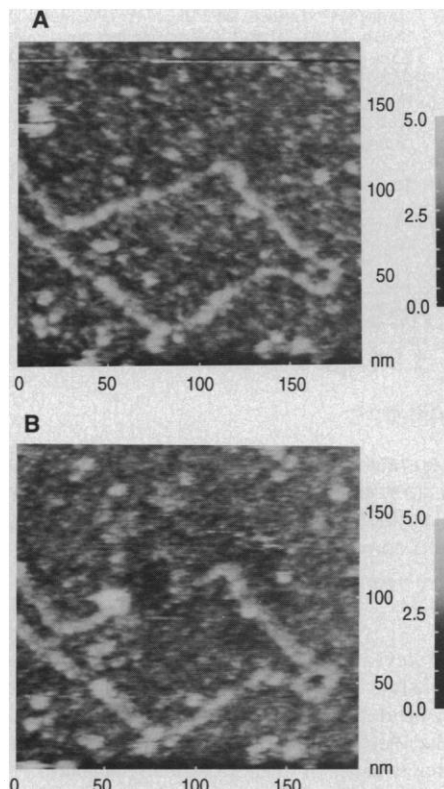
Fig. 5. Dissection of plasmids with the AFM. (**A**) and (**B**) are BlueScript II plasmid–imaged in propanol before (A) and after (B) scanning an area of ~30 nm by 30 nm at high force. Note upper region of plasmid that has been dissected away in (B). Plasmid width in (A) is 4 to 5 nm; in (B), after the high-force scan, evidence of a double tip is seen. Image sizes are 200 nm by 200 nm. The images have been processed only by flattening to remove background slope.

panied by 100,000 or more other DNA molecules on the mica square, and are distinguished from the other molecules only by their length. Force dissection has previously been used with gap junctions (20) to remove one layer of the double layer of junctions, thus revealing the extracellular surface of these junctions.

There has been a great deal of excitement in the field of scanning probe microscopy of DNA. Scanning tunneling microscope (STM) images have appeared to show the double helix (21), base pairs in the double helix (22), and the rings in adenine, thymine, guanine, and polyA (23). Many DNA-like artifacts have been observed, some of them published (24, 25). The particular concern about artifacts in STM of molecules on graphite (24, 26) is not a problem for AFM of DNA on mica or other insulating surfaces. Even on layered conducting substrates, such as graphite, the AFM is less sensitive than the STM to unusual electronic structure (27) and thus may not be affected by some of the STM artifacts. AFM of DNA on lipid films has

resolved features with the size and spacing of bases (28) and has even allowed the identification of a few bases (13), although not in an unambiguous and reproducible way. These experiments differed from those presented here with respect to substrate, solvent, and length of DNA. The early tantalizing ultrahigh-resolution AFM and STM images of nucleic acids lend support to the hope that such resolution can be obtained reliably with further advances in tip and sample preparation.

REFERENCES AND NOTES

1. G. Binnig, C. F. Quate, Ch. Gerber, *Phys. Rev. Lett.* **56**, 930 (1986).
2. D. Rugar and P. K. Hansma, *Phys. Today* **43**, 23 (1990).
3. G. Binnig et al., *Europhys. Lett.* **3**, 1281 (1987).
4. J. Vesenka et al., *Ultramicroscopy*, in press.
5. C. J. Bustamante et al., *Biochemistry* **31**, 22 (1992).
6. This variation of the method in (4) and (5) was used for some samples: Freshly cleaved mica soaked 4 to 24 hours in 33 mM magnesium acetate was sonicated 15 to 30 min in distilled water, dried with compressed air, glow-discharged for 20 s at 100 mtorr air, and inverted on a drop of DNA on Parafilm containing 50 to 300 ng of DNA in 10 to 30 μl of aqueous solution with an ionic strength of less than 1 mM; it was then rinsed, dried, and stored over desiccant. Good samples were sometimes, but not always, obtained when the glow-discharge step was omitted.
7. T. Koller, J. M. Sogo, H. Bujard, *Biopolymers* **13**, 995 (1974).
8. T. Kunisada and H. Yamagishi, *Plasmid* **9**, 8 (1983).
9. Digital Instruments, 6780 Cortona Drive, Santa Barbara, CA 93117.
10. T. R. Albrecht and C. F. Quate, *J. Vac. Sci. Technol. A* **6**, 271 (1988).
11. A. L. Weisenhorn, P. K. Hansma, T. R. Albrecht, C. F. Quate, *Appl. Phys. Lett.* **54**, 2651 (1989).
12. B. Drake et al., *Science* **243**, 1586 (1989).
13. H. G. Hansma et al., *J. Vac. Sci. Technol.* **9**, 1282 (1991).
14. W. Saenger, *Principles of Nucleic Acid Structure* (Springer-Verlag, New York, 1984); G. A. Jeffrey, *Hydrogen Bonding in Biological Structures* (Springer-Verlag, New York, 1991).
15. J. N. Israelachvili, *Intermolecular and Surface Forces with Applications to Colloidal and Biological Systems* (Academic Press, New York, 1985).
16. M. J. Allen et al., *Ultramicroscopy*, in press.
17. Y. Akama, E. Nishimura, A. Sakai, H. Murakami, *J. Vac. Sci. Technol. A* **8**, 429 (1990); D. Keller and C. Chih-Chung, *Surf. Sci.*, in press; K. L. Lee and M. Hatzakis, *J. Vac. Sci. Technol.* **7**, 1941 (1989).
18. M. J. Vasile et al., *Rev. Sci. Instrum.* **62**, 2167 (1991).
19. E. Henderson, *Nucleic Acids Res.*, in press.
20. J. H. Hoh, R. Lal, S. A. John, J.-P. Revel, M. F. Arnsdorf, *Science* **253**, 1405 (1991).
21. G. Lee et al., *ibid.* **244**, 475 (1989); S. M. Lindsay et al., *ibid.*, p. 1063; T. P. Beebe, Jr., et al., *ibid.* **243**, 370 (1989).
22. R. J. Driscoll et al., *Nature* **346**, 294 (1990); A. Cricenti et al., *Science* **245**, 1226 (1989).
23. M. J. Allen et al., *Scanning Microsc.* **5**, 625 (1991); D. D. Dunlap and C. Bustamante, *Nature* **342**, 204 (1989); W. M. Heckl et al., *Proc. Natl. Acad. Sci. U.S.A.* **88**, 8003 (1991); W. M. Heckl and J. F. Holzrichter, in *Nonlinear Optics* (Gordon and Breach, Singapore, 1992), vol. 1, pp. 53–59.
24. C. R. Clemmer and T. P. Beebe, Jr., *Science* **251**, 640 (1991).
25. W. M. Heckl and G. Binnig, *Ultramicroscopy*, in press.
26. C.-Y. Liu, H. Chang, A. J. Bard, *Langmuir* **7**, 1138 (1991).

27. J. Schneir, R. Sonnenfeld, P. K. Hansma, J. Ter-
    soff, *Phys. Rev. B* **34**, 4979 (1986).
28. A. L. Weisenhorn *et al.*, *Langmuir* **7**, 8 (1991).
29. We gratefully acknowledge scientific advice and
    valuable discussions with J. H. Hoh, A. Engel, J.
    N. Israelachvili, A. Weisenhorn, E. Henderson, K.
    Kjoller, and M. Amrein. We thank P. Russell for
    providing us with samples of his super tips, P.
    Petroff for use of his ion mill, J. Cleveland for

Fig. 1. Latitudinal distribution of lightning from space (5), showing a dominant contribution from the tropics (±23°).

The Schumann Resonance: A Global Tropical Thermometer

Earle R. Williams

The Schumann resonance, a global electromagnetic phenomenon, is shown to be a sensitive measure of temperature fluctuations in the tropical atmosphere. The link between Schumann resonance and temperature is lightning flash rate, which increases nonlinearly with temperature in the interaction between deep convection and ice microphysics.

Considerable interest has focused in recent years on temperature fluctuations in the earth's atmosphere. The global temperature variability, based on a century's surface (dry-bulb) temperature records, amounts to several tenths of 1°C (1–3). The reported global warming amounts to only a few tenths of 1% of the absolute temperature. Thus, it would be valuable to identify measurable physical parameters that are nonlinearly dependent on the fluctuations in atmospheric temperature so that some gain in the detection of these subtle temperature changes can be achieved. In this report I investigate the idea that the Schumann resonance, a global electromagnetic phenomenon driven by worldwide lightning activity, is one such measurable parameter. Lightning is linked with cloud electrification and the accumulation of ice particles in the upper troposphere. The nonlinear electrification process is controlled by buoyancy, the modest departures from hydrostatic equilibrium caused by temperature differences of the order of 1°C. Buoyancy in turn is controlled primarily by surface air temperature, the principal datum in current studies of global change.

Convection is systematically deeper and more frequent in the tropics than at higher latitudes. This behavior is essentially the result of the pole-to-equator temperature increase and the Clausius-Clapeyron relation. Lightning activity increases dramatically with the depth and vigor of convection (4) and is dominant in the tropics (5, 6) (Fig. 1). Approximately two of every three lightning flashes occur in the latitude interval ±23°.

Observations of lightning from space (5,

Department of Earth, Atmospheric, and Planetary Sciences, Massachusetts Institute of Technology, Cambridge, MA 02139.

6) reveal that tropical land areas exhibit substantially more lightning than do the central oceans. Southeast Asia and Australia, Africa, and South America are three major zones of deep electrically active convection. The land-ocean lightning contrast is attributable to small (a few degrees celsius) differences in the surface temperature over land and over the sea.

Lightning activity at a large number of land stations in the tropics increases nonlinearly with surface air temperature. In the following comparisons, wet-bulb temperature rather than dry-bulb temperature will be used, because the former records simultaneously the effect of temperature and moisture, both of which are important to the thermodynamics of moist convection. Many parameters in addition to surface temperature influence the development of deep convection and lightning on any given day and place (for example, temperature inversions, dry layers, wind shear, and lateral gradients in surface temperature). Consequently, a single-parameter (wet-bulb temperature in this case) relation with lightning flash count is variable on a day-to-day basis. When monthly mean values are considered, however, a consistent association between lightning and temperature emerges and the data show reasonably well-defined seasonal variations. For example, data from within ~50 km of Darwin, Australia (12°S), show (Fig. 2) that monthly mean lightning counts (7, 8) increased more than two orders of magnitude as the wet-bulb temperature increased from 25° to 27°C (the monthly mean of maximum daily values). Lightning activity reached a maximum during the wet season months (November through March).

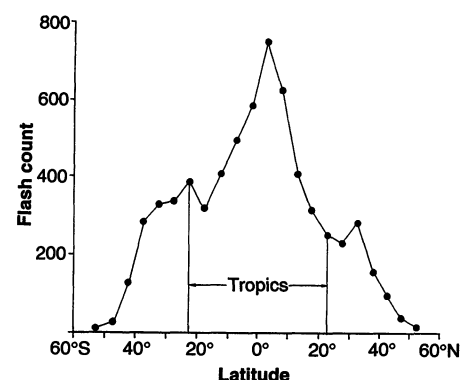Observations from Kourou, French Guiana (5°N), South America (9), show a

similar strong sensitivity (Fig. 3). This site, closer to the equator than Darwin, experiences a smaller annual variation in wet-bulb temperature, but a modest 1.9°C annual change was associated with a 20-fold change in lightning activity.

At latitudes more distant from the equator but still within the tropics, the annual variation of wet-bulb temperature increased while the annual variation of monthly mean lightning activity remained about the same. Consequently, the lightning sensitivity to seasonal variations in temperature decreases with increasing latitude. Data from Mexico (10), southern Brazil (11), and Botswana in Africa (12) show approximate doublings of lightning activity per 1°C of wet-bulb temperature change. In Orlando, Florida (28°N), which lies outside the tropical belt but is the most lightning-active region in the United States, a similar sensitivity has been observed (13) (Fig. 4).

The interpretation of the sensitive relation between lightning and wet-bulb temperature is based on observations of the thermodynamic structure of the tropical
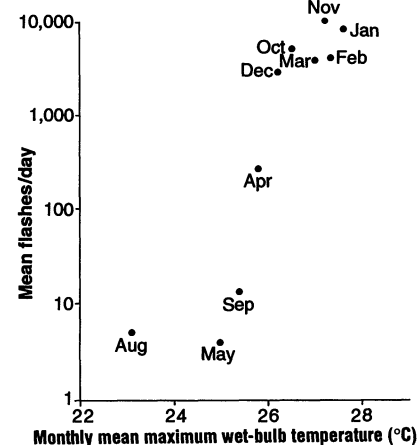

Fig. 2. Monthly lightning counts (7) for Darwin, Australia (12°S), versus monthly mean maximum wet-bulb temperature for 1988.